Low Cyclic Fatigue Behavior of Alloy 625 at Ambient and Elevated Temperatures

Mubashir Bashir, R. Kannan, R. Sandhya and G. A. Harmain

Abstract Nickel base superalloy, alloy 625 is chosen to be the candidate material for the casing of the rotor in the Advanced Ultra Supercritical (AUSC) power plant, being developed in India. The casing of the rotor is subjected to repeated thermal stresses as a result of temperature gradients that occur on heating and cooling during start-ups and shutdowns or during temperature transients that leads to the Low-Cycle Fatigue (LCF) deformation. The present study deals with LCF behavior of the alloy 625. LCF tests were conducted on the alloy in the temperature range 300–973 K at strain amplitudes in the range $\pm$ 0.25 to $\pm$ 1%, employing a constant strain rate of 3×10^{-3} s^{-1} using a completely reversed (R = −1) triangular waveform on a servo-electric fatigue machine as per ASTM E606. The cyclic stress response of the alloy was characterized by a continuous hardening before the onset of failure under all testing conditions. The fatigue life was found to decrease with an increase in the test temperature and the applied strain amplitude. Dynamic Strain Aging is found to influence the fatigue deformation of the alloy and was characterized by the serrations in the stress–strain hysteresis loops, a negative dependence of half-life stress amplitude and plastic strain amplitude. The results obtained are correlated with the detailed optical and scanning electron microscopic investigations.

Keywords Alloy 625(as-cast) · Low cycle fatigue · DSA · Cyclic stress response

M. Bashir · G. A. Harmain
Department of Mechanical Engineering, NIT Srinagar, Srinagar, India

R. Kannan (✉) · R. Sandhya
Metallurgy and Materials Group, Indira Gandhi Centre for Atomic Research, 603102 Kalpakkam, TN, India
e-mail: rkannan@igcar.gov.in

R. V. Prakash et al. (eds.), *Structural Integrity Assessment*, Lecture Notes in Mechanical Engineering, https://doi.org/10.1007/978-981-13-8767-8_55

1 Introduction

Alloy 625 is a nickel base solid solution strengthened superalloy having good combinations of high-temperature mechanical properties, microstructural stability, corrosion/oxidation resistance, good castability, significant damping resistance as well as excellent creep and fatigue resistance [1, 2]. The castability is difficult to achieve with precipitation strengthened alloys having high Ti and Al alloying elements, however, Europe has gained a success to produce the solid solution strengthened alloy with good castability [3]. The high strength and good thermal stability of equiaxed cast alloy are attributed to: solid solution strengthening with additions of refractory alloying elements such as Mo and Nb, strengthening of grain boundaries by carbides, precipitation strengthening by γ' precipitate [Ni_3 (Al, Ti)] due to the addition of Al and Ti. Moreover, the addition of Nb leads to strengthening by precipitation of metastable γ'' phase [Ni_3 (Nb, Al, Ti)] [4, 5]. The top priority of indigenous AUSC power plant is material development for the design of various components to provide highly efficient, highly reliable, affordable, and environment-friendly electricity. Alloy 625 is treated as the most potential candidate material for the complex casing of AUSC turbine rotor. The casing of the rotor encounters intermittent thermal stresses as a result of temperature gradients that occur on heating and cooling during start-ups and shutdowns or fluctuating temperature transients during the service, that introduces the low-cycle fatigue (LCF) deformation. Hence, in the present study, LCF tests have been conducted on Alloy 625 in the cast form. The material has exhibited cyclic hardening and DSA phenomena. The casting defects introduce a significant scatter in LCF data.

2 Experimental

The 100 mm × 11 mm × 11 mm rectangular blanks were taken out from as-received cast block, from which cylindrical specimens of 6 mm gauge diameter and 12.5 mm gauge length was machined out. The chemical composition of nickel base superalloy, alloy 625 (as-cast) used in this investigation is shown in Table 1. LCF tests were performed in air, using a servo-electric fatigue testing machine equipped with a high-temperature furnace. The axial strain controlled LCF tests were carried out as per ASTM E606. The LCF tests were conducted at various strain amplitudes ranging from $\pm$ 0.25% to 1% at 300, 573, 873, and 973 K, employing triangular waveform with a constant strain rate of 3×10^{-3} s^{-1}.

Table 1 Chemical composition of alloy 625, wt%

Elements	P	S	C	Mn	Si	Al	Ti	Fe	Nb	Mo	Cr	Ni
wt.%	0.005	0.007	0.02	0.17	0.18	0.18	0.19	2.86	3.53	8.63	21.34	Bal.

Metallographic examination was done on tested and untested specimens using electrolytic etching (10% perchloric acid in methanol) for 3 min. Fractography of the failed samples were studied in a scanning electron microscope.

3 Results and Discussion

3.1 Microstructure

The initial microstructure of alloy 625 is shown in Fig. 1. The grain boundary was not visible as the grain was quite big. However, the micrograph clearly shows dendritic structure with Nb and Mo interdendritic dark field [3]. Optical micrograph of the tested specimen showed carbides and precipitates both within grains and along the grain boundaries (Fig. 2).

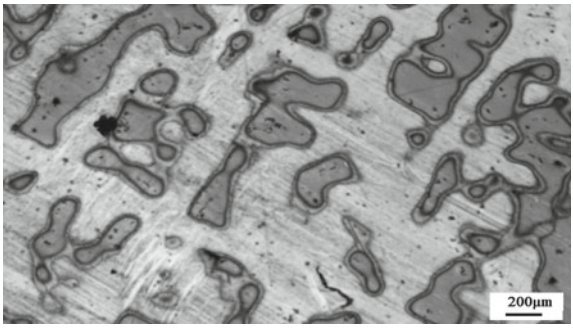

Fig. 1 Initial microstructure of alloy 625

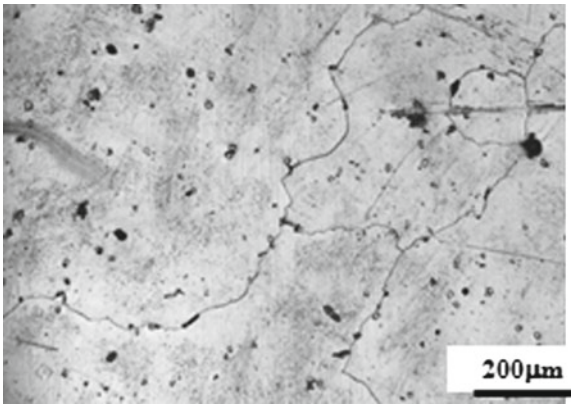

Fig. 2 Micrograph of the tested sample

3.2 *Cyclic Stress Response Behavior*

3.2.1 Effect of Strain Amplitude

The cyclic stress response of alloy 625 with the change in applied strain amplitude for a given temperature is portrayed in Fig. 3a–d. The general observation is that there is a continuous increase in the stress values from the first cycle onwards followed by a drastic decrease in the same due to initiation and propagation of macrocracks. There is an overall upward shift of CSR curves with an increase in strain amplitude at all four temperatures. The cyclic hardening in alloy 625 can be attributed to (a) dislocation multiplication and accumulation within the slip band [6], (b) heterogeneous precipitation of fine $M_{23}C_6$ carbides at the dislocations [7], (c) in situ precipitation of γ' and (d) dislocation and solute atom interactions (dynamic strain aging, DSA).

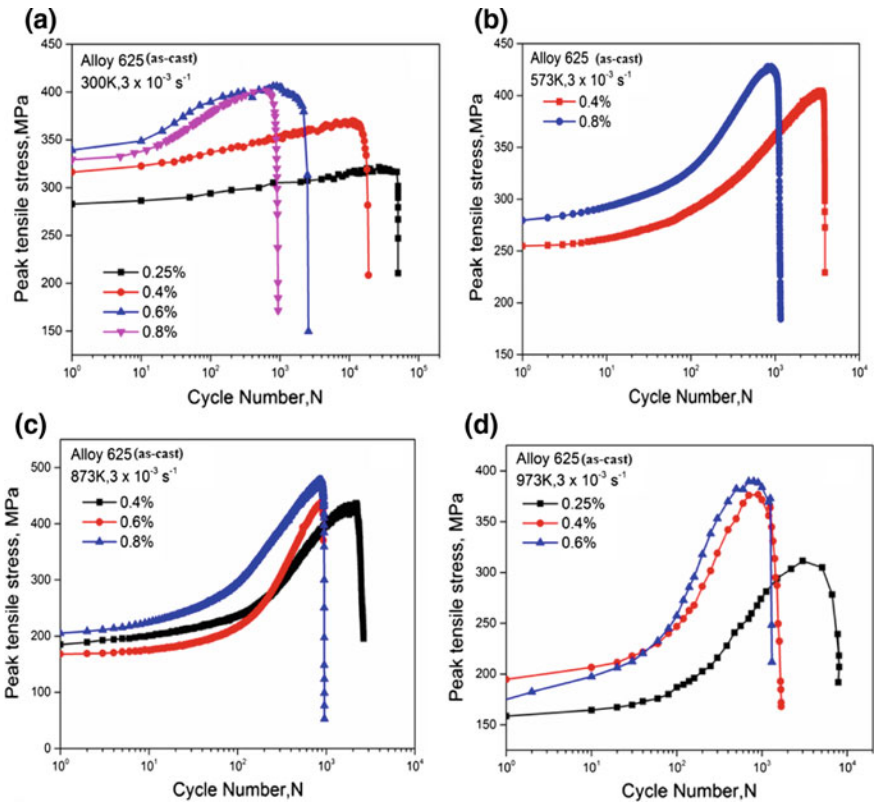

Fig. 3 Effect of strain amplitude on the cyclic stress response of alloy 625 at **a** 300 K, **b** 573 K, **c** 873 K and **d** 973 K

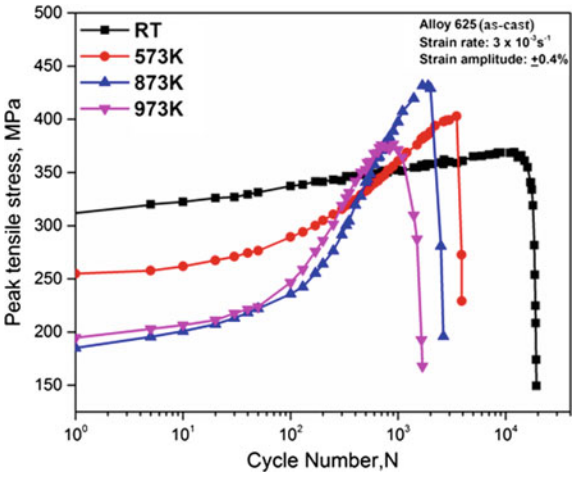

Fig. 4 Effect of temperature on the cyclic stress response of alloy 625 at strain amplitude of ±0.4%

3.2.2 Effect of Temperature

Figure 4 illustrates the cyclic stress response as a function of temperature for a constant strain amplitude (±0.4%). It has been observed that the cyclic hardening increases linearly at 300 K whereas at higher temperatures the increase is steep until failure. It has been observed that peak tensile stress decreases with increase in temperature during the initial part of cycling, typically, about 100 cycles. At higher number of cycles the stress response is higher for higher temperatures, showing a steep hardening effect, in comparison to 300 K. These observations point to the fact that there is a difference in the underlying deformation mechanisms under different temperature–strain amplitude combinations that affect the cyclic stress response of alloy 625.

Figure 5 shows the Coffin–Manson plot for alloy 625 at different temperatures and the parameters obtained from the linear regression method are given in Table 2. The slope of Coffin–Manson plot is sharper at 873 K and above, indicating greater damage in the material leading to the lowering of fatigue life at these temperatures.

3.3 Dynamic Strain Aging and Its Manifestations During Low-Cycle Fatigue Deformation

In the present study, serrations have been observed in the plastic portions of stress–strain hysteresis loops at a strain amplitude of ±0.6% and at temperatures 873 and 973 K, shown in Fig. 6a, b and the plastic portions are enlarged in Fig. 7a, b. This has been attributed to the occurrence of DSA. However, the absence of serrations in hysteresis loops does not imply absence of DSA [8]. Furthermore, the anomalous stress response, i.e. increase in cyclic stress with an increase in temperature has

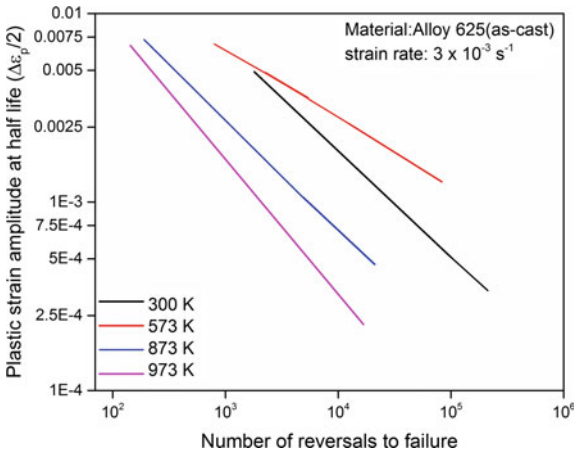

Fig. 5 Coffin–Manson plot of alloy 625 tested at various temperatures

Table 2 Effect of temperature on Coffin–Manson constants for alloy 625

Temperature, K	Fatigue ductility coefficient, ε_f'	Fatigue ductility exponent, c
300	0.3364	−0.5638
573	0.0754	−0.3551
873	0.1644	−0.5941
973	0.2369	−0.7157

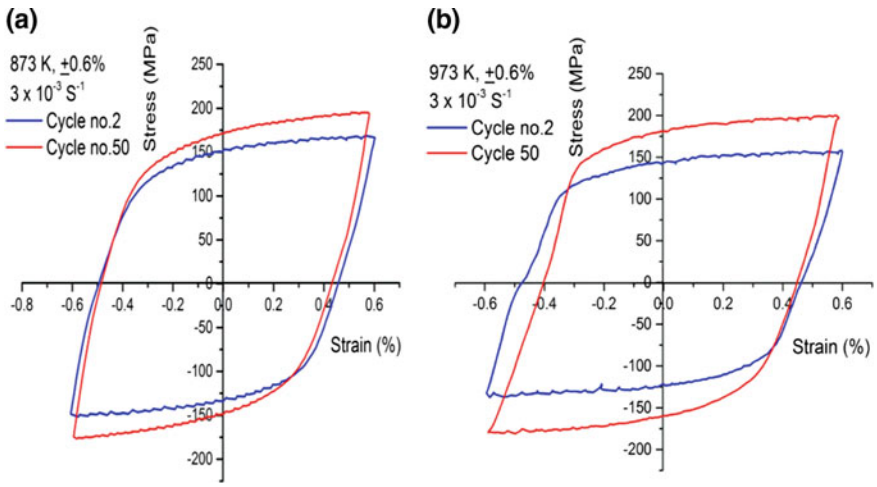

Fig. 6 Representation of the evolution of hysteresis loops at **a** 873 K and **b** 973 K

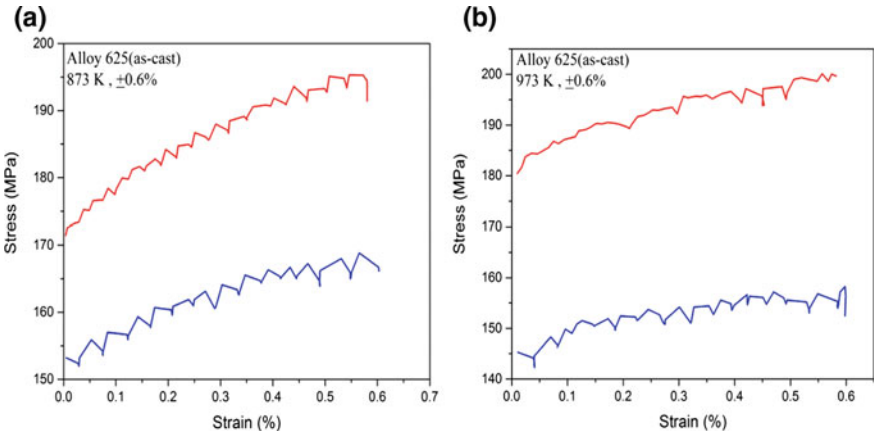

Fig. 7 Serrations observed in alloy 625 in stress–strain hysteresis loops at **a** 873 K and **b** 973 K

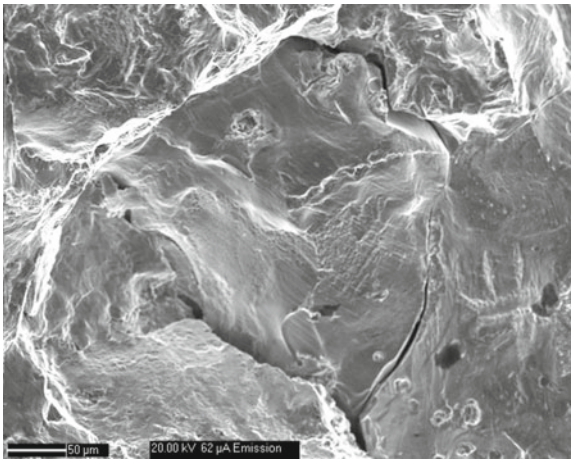

Fig. 8 SEM fractograph of the sample tested at 973 K and at a strain amplitude of ±0.4% showing extensive oxidation of the fracture surface

been observed at temperatures of 873 and 973 K. While serrations are present at 973 K, the effect of DSA does not seem to be very predominant at this temperature. The hardening at 973 K could have a contribution from precipitation. DSA fundamentally results from attractive interaction between solute species and mobile dislocations, either during their glide [9] or temporary arrest at local obstacles in the glide plane [10]. Consequently, the unlocking of dislocations or generation of new dislocations results in increased stress response, for maintaining the imposed strain.

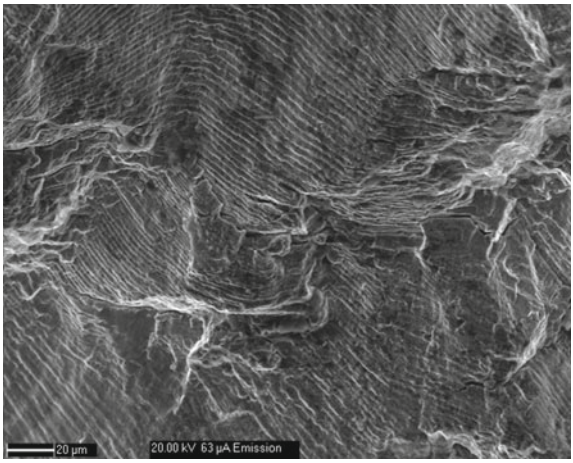

Fig. 9 SEM fractograph of the sample tested at 973 K and at a strain amplitude of ±0.4%

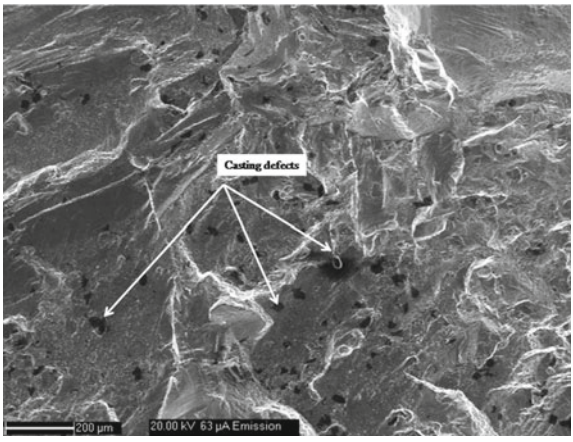

Fig. 10 SEM fractograph of the sample tested at 873 K and at a strain amplitude of ±0.4% showing extensive casting defects (Shrinkage Cavities)

3.4 Fractographic Studies

The effect of oxidation leading to lower life can be clearly seen at 973 K, Fig. 8. As seen from the representative fractography in Fig. 9, the fatigue failure was typically by transgranular mode evidenced by striations on the fracture surface. The scatter in the LCF properties can be attributed to the casting defects as is evident in Fig. 10.

4 Conclusions

1. alloy 625 exhibited intense cyclic hardening at all temperatures of investigation and the rate of hardening is more at 873 and 973 K.
2. LCF life decreased with increase in temperature and strain amplitude.
3. Evidence for the operation of dynamic strain aging was obtained in the form of serrations, increased hardening and a minima in the plastic strain. The peak DSA temperature in the range of temperatures studied was 873 K.
4. The fracture mode was predominantly transgranular, as evidenced by striations on the fracture surface. Oxidation also played a role in the fracture at 973 K.
5. It was shown that the scatter in the LCF properties can be attributed to the casting defects (shrinkage cavities) present in the material, as observed by scanning electron microscopy.

References

1. J.M. Rakowski, C.P. Stinner, M. Lipschutz, J.P. Montague, E.A. Loria (eds.), *The Minerals, Metals and Materials Society* (2005), pp. 271–286
2. L.E. Shoemaker, E.A. Loria (eds.), *The Minerals, Metals and Materials Society* (2005), pp. 409–418
3. W. Yu, S. Liu, Y. Wang, L. Sun, *Energy Materials* (2017), pp. 213–223
4. C. Yuan, X. Sun, Fengshi Yin, Y. Yu, J. Mater. Sci. Technol. **17**, 425–428 (2001)
5. A. Nagesha, P. Parameswaran, Niraj Kumar, R. Sandhya, M.D. Mathew, Mater. High Temp. **29**, 49–53 (2012)
6. G. Chai, P. Liu, J. Srodigh, Mater. Sci. **39**, 2689 (2004)
7. W.l. Mankins, J.C. Hosier, T.H. Bassford, Microstructure and phase stability of Inconel 617. Metall. Trans. **5**, 2579–2590 (1974)
8. K.K. Ray, K. Dutta, S. Sivaprasad, S. Tarafder, Procedia Eng. **2**, 1805–1813 (2010)
9. A.H. Cottrell, *Oxford University, London* (1953)
10. A.W. Sleeswyk, Acta Metall. **6**, 598–603 (1958)